Observation of a Low-Lying Metastable Electronic State in Highly Charged Lead by Penning-Trap Mass Spectrometry

Kathrin Kromer,[1,*] Chunhai Lyu,[1] Menno Door,[1] Pavel Filianin,[1] Zoltán Harman,[1] Jost Herkenhoff,[1] Paul Indelicato,[2] Christoph H. Keitel,[1] Daniel Lange,[1] Yuri N. Novikov,[3,4] Christoph Schweiger,[1] Sergey Eliseev,[1] and Klaus Blaum[1]

[1]*Max-Planck-Institut für Kernphysik, 69117 Heidelberg, Germany*
[2]*Laboratoire Kastler Brossel, Sorbonne Université, CNRS, ENS-PSL Research University, Collège de France, Paris, France*
[3]*Department of Physics, St Petersburg State University, St. Petersburg 198504, Russia*
[4]*NRC "Kurchatov Institute"-Petersburg Nuclear Physics Institute, Gatchina 188300, Russia*

(Received 21 April 2023; revised 9 October 2023; accepted 17 October 2023; published 29 November 2023)

Highly charged ions (HCIs) offer many opportunities for next-generation clock research due to the vast landscape of available electronic transitions in different charge states. The development of extreme ultraviolet frequency combs has enabled the search for clock transitions based on shorter wavelengths in HCIs. However, without initial knowledge of the energy of the clock states, these narrow transitions are difficult to be probed by lasers. In this Letter, we provide experimental observation and theoretical calculation of a long-lived electronic state in Nb-like Pb^{41+} that could be used as a clock state. With the mass spectrometer PENTATRAP, the excitation energy of this metastable state is directly determined as a mass difference at an energy of 31.2(8) eV, corresponding to one of the most precise relative mass determinations to date with a fractional uncertainty of 4×10^{-12}. This experimental result agrees within 1σ with two partially different *ab initio* multiconfiguration Dirac-Hartree-Fock calculations of 31.68(13) eV and 31.76(35) eV, respectively. With a calculated lifetime of 26.5(5.3) days, the transition from this metastable state to the ground state bears a quality factor of 1.1×10^{23} and allows for the construction of a HCI clock with a fractional frequency instability of $< 10^{-19}/\sqrt{\tau}$.

DOI: 10.1103/PhysRevLett.131.223002

The invention of the frequency comb [1,2] opened up the possibility to use optical transitions as frequency standards, called optical atomic clocks. These clocks, using single ions in Paul traps [3,4] or arrays of atoms in optical lattices [5,6], have reached incredible fractional frequency instabilities of below $2 \times 10^{-16}/\sqrt{\tau}$ for individual optical clocks [7], τ being the averaging time, and $5 \times 10^{-18}/\sqrt{\tau}$ for spatially separated atomic ensembles [6]. This extremely high precision not only provides a standard for frequency measurements, it also enables the search for physics beyond the standard model, such as temporal or spatial variation of fundamental constants [8,9] or violations of Einstein's equivalence principle through tests of local position invariance [10]. It is therefore of great importance to push this precision frontier even further to be able to limit the possible size of these effects. One way of achieving this would be to go to strongly forbidden atomic transitions in the extreme ultraviolet (XUV) region.

With a new generation of frequency combs now spanning more than the optical range and reaching up to the XUV [11–16], research into matching transitions has intensified. Transitions in highly charged ions (HCIs) have become of interest for a new generation of clocks [17–19]. Though these clocks usually do not hold appropriate transitions for laser cooling and state readout, they can be interrogated via quantum logic spectroscopy [20], which has been demonstrated in highly charged Ar^{13+} with a fractional instability of $3 \times 10^{-14}/\sqrt{\tau}$ for an optical clock transition [21].

HCI transitions are widely shielded from field-induced frequency shifts. The remaining electrons of HCIs are bound orders of magnitude stronger than the corresponding electrons in a neutral atom or singly charged ion, making the influence of external fields as well as blackbody radiation minimal [22,23]. However, the frequency of a coherent laser usually has a limited tuning range, and a metastable state has a narrow transition. Without initial knowledge of the energy of the clock state, it is difficult to design a direct laser-spectroscopy experiment of the clock transition. High-precision mass spectrometry thus provides

an alternative approach to infer the energy of a long-lived clock state and, at the same time, to test state-of-the-art theoretical calculations.

In this Letter, with the Penning-trap mass spectrometer PENTATRAP and the multiconfiguration Dirac-Hartree-Fock (MCDHF) theory, we present the experimental observation and the theoretical calculation of a low-lying metastable electronic state in Nb-like $^{208}Pb^{41+}$. The excitation energy is determined to be around 31 eV with sub-eV uncertainty. Unlike previous mass-spectroscopy measurements of a metastable state around 200 eV in Re^{29+} [24], this metastable state can be effectively probed via available XUV frequency combs, rendering it more feasible to construct an XUV clock. With a calculated lifetime of 26.5(5.3) days, such a clock bears a quality factor of 1.1×10^{23}. Assuming a clock interrogation linewidth of 1 mHz available for optical lasers [25], such an XUV clock could achieve a fractional frequency instability of around $4 \times 10^{-20}/\sqrt{\tau}$. Similar clock states can also be scaled to higher and lower transition energies by employing different elements of the Nb-like isoelectronic sequence [19].

To produce highly charged ions, a Heidelberg compact electron beam ion trap (EBIT) [26] equipped with an in-trap laser desorption setup is used [27]. Inside this table-top-sized EBIT, a few-keV electron beam is produced and then guided and compressed by permanent magnets to ionize atoms and ions to high charge states by electron impact ionization. A target made of ^{208}Pb, positioned next to the trap center, is used as a source of neutral material. By aiming a pulsed Nd:YAG laser with a pulse energy and duration of about 0.5 mJ and 8 ns, respectively, at the target, a small amount of target material is evaporated into the trap region. In a process called "charge breeding," the ions remain trapped inside the central drift tube, which is set to a depth of 20 V compared to the neighboring drift tubes of the EBIT and reach higher and higher charge states by electron impact ionization until they arrive at an equilibrium charge distribution. During electron-ion interaction processes inside the EBIT's ion plasma, such as electron impact excitation or radiative or dielectronic recombination, some of the ions' electrons become highly excited [28]. After the short-lived excited states decay cascadingly, a fraction of the HCIs will remain in long-lived states for an extended period of time. This fortuitous population of the metastable state allows us to measure the excitation energy of the metastable state without having to actively drive the transition by using mass measurements. This method does not require prior knowledge of the state energies, which makes these measurements independent of theory or other experiments.

The HCIs are extracted from the EBIT and slowed down from 4 keV/q to a few eV/q to be able to trap them in a cryogenic Penning trap. The ion transport at the experiment PENTATRAP works via an electrostatic beamline in combination with a Bradbury Nielson gate [29] for charge state selection. The ions are then decelerated by a set of two pulsed drift tubes, one of which is situated in the room temperature region (deceleration down to ≈200 eV/q) and a second one in the cryogenic part of the beamline (down to a few eV/q) and ultimately captured in the first Penning trap. For an overview of the beamline setup, see Ref. [30].

To determine mass ratios of stable or long-lived highly charged ions, five identical, aligned, cylindrical Penning traps are used in PENTATRAP's trap tower [see Fig. 1(a)] [31,32]. The trap tower opens the possibility to conduct simultaneous measurements on two ions stored in Traps 2 and 3 while having two more traps for ion storage. The fifth trap is currently not in use. The measurement principle is based on a measurement of the frequencies of the ions' three Penning-trap eigenmotions: the modified cyclotron frequency ν_+, the axial frequency ν_z, and the magnetron frequency ν_- and calculating the free cyclotron frequency $\nu_c = qB/(2\pi m)$ by applying the invariance theorem [33]

$$\nu_c = \sqrt{\nu_+^2 + \nu_z^2 + \nu_-^2}. \tag{1}$$

The free cyclotron frequency ν_c is inversely proportional to the mass m of the ion and proportional to the exactly known charge q of the ion and the magnetic field B. In order to achieve a precise determination of the mass of the ion in the excited electronic state m_{exc}, the cyclotron frequency of an ion in the ground state $\nu_{c,\mathrm{g}}$ is measured alternately to that of an ion in the excited state $\nu_{c,\mathrm{exc}}$ in each of the measurement traps. When determining the ratio $R = \nu_{c,\mathrm{g}}/\nu_{c,\mathrm{exc}}$ for Trap 2 or Trap 3 of the two cyclotron frequencies, the magnetic field, being the least precisely known quantity, cancels out to first order and the identical charge of both ions drops out of the ratio. The mass difference Δm between the ion in the ground state m_{g} and the excited state m_{exc} can then be determined with

$$\Delta m = m_{\mathrm{exc}} - m_{\mathrm{g}} = m_{\mathrm{g}}(R-1). \tag{2}$$

The individual ions in each measurement trap [see Fig. 1(a)] are detected nondestructively using the Fourier-transform ion-cyclotron-resonance technique [34]. This well-established method uses the ion's image current, which is converted into a measurable voltage drop across a resonant tank circuit at cryogenic temperatures. When the cryogenic tank circuit is connected to an axially offset electrode, one can reduce the amplitude of the axial motion by thermalizing it, and measure its frequency as a "dip" in the resonance curve [34]. By coupling the modified cyclotron or the magnetron motion to the axial motion, the coupled motion is cooled and its frequency can be measured using the double-dip technique [35]. This technique is applied to determine the magnetron frequency and for estimating frequencies and coupling pulse times for the phase-sensitive pulse and phase (PnP) method used in the main measurements [36]. A PnP cycle works as follows: in

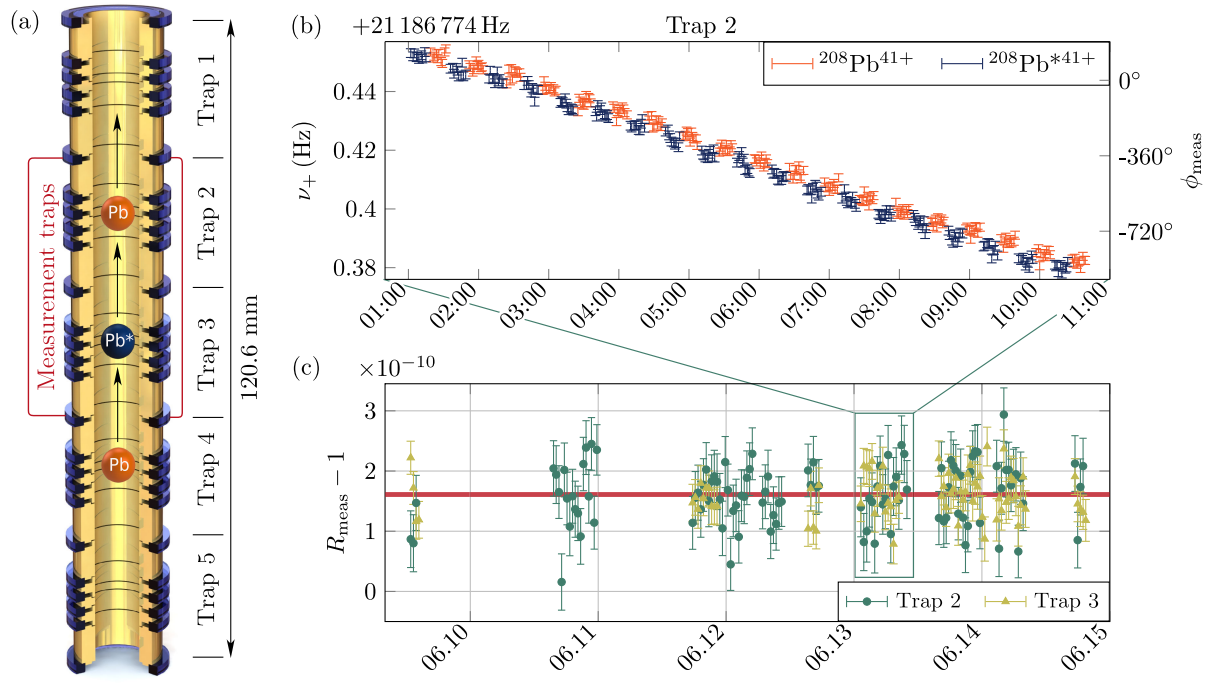

FIG. 1. (a) Schematic drawing of the Penning-trap tower with three ions in Configuration 1. The ion transport to Configuration 2 is implied by arrows. The phase measurements are carried out in Traps 2 and 3. Traps 1 and 4 are utilized as storage traps and Trap 5 is currently not in use. (b) Example of ν_+ data from a measurement in Trap 2 with $^{208}Pb^{41+}$ ions, one being in the ground state (orange) and one in the metastable state (blue). On the left y axis, the resulting frequency is shown while on the right y axis, the unwrapped, measured phase ϕ_{meas} is given. When combining the averaged modified cyclotron frequency with the axial and magnetron frequencies [see Eq. (1)], one can calculate the cyclotron frequencies and their ratios R plotted below in subfigure (c). This plot shows the ratios of all relevant measurement runs in both traps. The red line gives the average and its width corresponds to the combined statistical and systematic error band.

the beginning, the cyclotron motion is excited using a dipolar radio frequency (rf) pulse to set a specific starting phase; then the ion's cyclotron oscillation is left to evolve freely for a well-known time t_{acc}, called phase accumulation time. The energy and phase information of the cyclotron mode is then coupled to the axial mode using a π pulse at the sideband frequency $\nu_{rf} = \nu_+ - \nu_z$. Subsequently, the cyclotron phase information can be read out using the axial image-current detection system. With this method, one can distinguish between the ground state and low-lying metastable state in $^{208}Pb^{41+}$ (see Fig. 2). At a phase accumulation time of $t_{acc} = 40$ s the phase difference between metastable and ground state of about 49° at $\nu_+ \approx 21.2$ MHz exceeds the phase stability of about 12° [see Fig. 1(b)].

Once there are three ions loaded and identified in the alternating configuration shown in Fig. 1(a), the PnP measurement loop is started. In addition to the prior mentioned phase measurement, this also includes an axial frequency measurement during the phase accumulation time of the modified cyclotron frequency and a single magnetron frequency measurement in the preparation phase of the measurement. During the continuous PnP measurement loop, the ions are moved up or down every 10 measurement points to alternate between Configurations 1 and 2 effectively swapping the ions in each measurement trap from the ion in the ground state to the ion in the excited state or vice versa (see Fig. 1). For further information on the measurement procedure, see Refs. [24,30,37,38].

In the analysis, all three measured eigenfrequencies are combined, following Eq. (1), and the cyclotron frequency

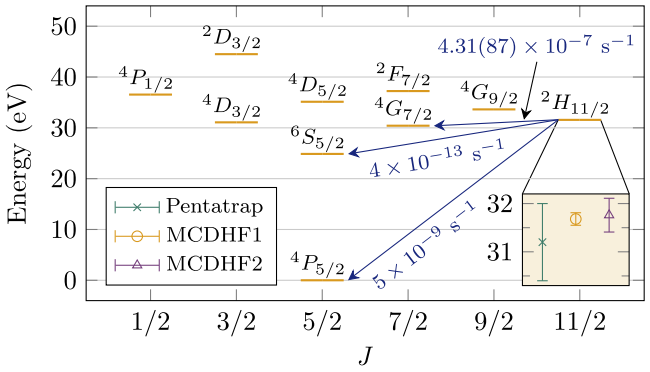

FIG. 2. Lowest energy levels of the Nb-like Pb^{41+} ion. The metastable $[Kr]4d^5\,{}^2H_{11/2}$ state lies at around 31 eV above the $[Kr]4d^5\,{}^4P_{5/2}$ state. It decays mainly via an $E2$ transition to the short-lived state $[Kr]4d^5\,{}^4G_{7/2}$. The metastable state has a lifetime of 26.5(5.3) days.

ratio is formed by interpolation, whereby one of the ion's block of 10 cyclotron frequency measurements is averaged and interpolated to the time of the other ion's averaged cyclotron frequency measurement. In Fig. 1(b) it is clearly visible that the modified cyclotron frequency ν_+ drifts downward by $\delta B/B = -2.3 \times 10^{-10}/\mathrm{h}$ due to a loss of magnetic field of the superconducting magnet. With the interpolation, this magnetic field drift is canceled out to first order.

The resulting ratios of both traps can be found in Fig. 1(c). The average ratio of all measurement runs was determined to be $R_{\mathrm{stat}} - 1 = 1.609(32) \times 10^{-10}$. Because of the almost identical charge-to-mass ratio of the ion in ground and metastable state, most known systematic effects, such as the image charge shift or the relativistic shift, cancel out to a large extent when forming the frequency ratio. Only one systematic uncertainty of relevant size remains, namely the dip line-shape uncertainty [39]. This systematic originates from the uncertainty of the axial dip frequency relative to the fitted resonator frequency. In Trap 3, the Q factor of the resonator is substantially larger and thus the dip width is substantially broader than in Trap 2, which increases the uncertainty of the resonator frequency because the center of the resonance spectrum is "covered" by the broad dip. As expected, the fit of the dip in Trap 3 yields a larger systematic error associated with the mismatch of the dip and resonator frequencies connected to the distortion of the dip shape due to the frequency pulling effect. These two effects in Trap 2 and Trap 3 result in an error of $< 1 \times 10^{-12}$ and 3.3×10^{-12}, respectively. Including this systematic effect, the final experimental mass ratio is determined to be $R - 1 = 1.61(4) \times 10^{-10}$. The mass or energy difference of the two states can then be calculated using Eq. (2) to be 31.2(8) eV. This small energy difference was measured as a relative mass measurement against the total mass of the Pb ion of $\approx 194\ \mathrm{GeV/c^2}$, reaching a relative precision of 4×10^{-12}.

The level structure and lifetimes of the low-lying states in Pb^{41+} (see Fig. 2), are calculated with the *ab initio* multiconfiguration Dirac-Hartree-Fock (MCDHF) and relativistic configuration interaction (RCI) methods in two partially different implementations, one of them being the GRASP2018 code [40–42] (referred to henceforth as MCDHF1) and the second one based on the Multiconfiguration Dirac-Fock with General Matrix Elements code [43] (referred to as MCDHF2). With a ground state of $[\mathrm{Kr}]4d^5\,{}^4P_{5/2}$, the metastable state is determined to be ${}^2H_{11/2}$.

Within the calculations of MCDHF1, each many-electron atomic state function is expanded as a linear combination of configuration state functions (CSFs) with common total angular momentum (J), magnetic (M), and parity (P) quantum numbers: $|\Gamma PJM\rangle = \sum_k c_k |\gamma_k PJM\rangle$. The CSFs $|\gamma_k PJM\rangle$ are jj-coupled Slater determinants of one-electron orbitals and γ_k summarizes all the remaining information needed to fully define the CSF, i.e., the orbital occupation and coupling of single-electron angular momenta. Γ collectively denotes all the γ_k included in the representation of the atomic state function.

In the calculation of the excitation energy of the $J = 11/2$ metastable state, the CSF basis set is generated via single and double (SD) excitation of electrons from the $4s^2 4p^6 4d^5$ reference configurations to high-lying virtual orbitals. After obtaining the radial wave functions from the self-consistent MCDHF calculations under the Dirac-Coulomb Hamiltonian, the RCI method is applied to derive the mixing coefficients c_k and excitation energies, as well as the approximate corrections arising from the mass shift, quantum electrodynamic (QED) terms, and Breit interaction.

To monitor the convergence of the result, we systematically added and optimized virtual orbitals layer by layer up to $n = 8$ with all orbital quantum numbers ranging from 0 to $n - 1$ being included (n is the principal quantum number). Through extrapolation to $n = \infty$, one obtains an energy of 31.672 eV within the calculation of MCDHF1 with 8.92×10^6 CSFs, which includes a 837 meV contribution from the Breit interaction, 47.2 meV from the self-energy correction, 0.07 meV from the vacuum polarization, 1.72 meV from the field shift, and 0.24 meV from the mass shift. The RCI calculations based on different radial wave functions lead to a correction of 6 meV. By varying the fine-structure constant in the calculation, this transition is found to have an α-variation sensitivity of $K = (\Delta E/E)/(\Delta\alpha/\alpha) = -1.74$. Considering the 10 times greater transition energy, the absolute frequency change due to α variations is comparable to other HCI candidates.

Furthermore, to account for the core-core correlations, the CSFs generated via SD excitations from the $1s$ orbital up to $5g$ orbital are added to the RCI calculations. This gives rise to a correction of -20 meV to the previous value. Then, through further inclusion of SD excitations from multireference $\{4s4p^64d^6, 4p^64d^7, 4s^24p^44d^7\}$ configurations up to the $6h$ orbital, the contribution from dominant triple and quadruple electron exchanges is considered in the RCI procedure with 13.7×10^6 CSFs. This gives a correction of 14 meV from high-order electron correlations. The final excitation energy is determined to be 31.68(13) eV. The uncertainty is conservatively given as the absolute summation of the corrections from the core-core and high-order correlations, the radial wave function dependence, plus 10% uncertainty from the Breit and QED terms.

The approach of MCDHF2 deviates from the above described calculations in the following way: in contrast to the perturbative approach of MCDHF1, the calculation within MCDHF2 includes the Breit and retardation term of the electron-electron interaction to all order by adding it directly to the many-body Hamiltonian. A smaller set of configurations is used compared to MCDHF1, but

including a full relaxation of all orbitals. Single, double, and triple excitations were limited to excitations from the $n = 4$ shell: $4s$, $4p$, $4d$ to $4d$, $4f$, $5s$, $5p$, $5d$,$6s$, $6p$ with approximately 29 000 configurations for the $^2H_{11/2}$ state and 24 000 configurations for the ground state. For the self-energy screening, two different methods are used [44–46] and more high-order QED corrections are included; however, the contribution of this is minimal for the case of transition energies in Pb^{41+}. The MCDHF2 method reaches a final value for the excitation energy of 31.76(35) eV, in excellent agreement with the MCDHF1 result.

While the metastable state decays to the ground state via a magnetic octupole ($M3$) transition under a rate of $A_1 = 4.95(5) \times 10^{-9}\ \mathrm{s}^{-1}$, its lifetime is mainly determined by the electric quadropole ($E2$) decay channel to the $J = 7/2$ state (see Fig. 2). The decay rates were calculated with the MCDHF1 method. Under the above mentioned multireference scheme, we expanded the CSF basis set to $n = 8$ and obtained a rate of $5.18 \times 10^{-7}\ \mathrm{s}^{-1}$ and $4.31 \times 10^{-7}\ \mathrm{s}^{-1}$ in the Coulomb and Babushkin gauge, respectively. Since both rates show decreasing trends with n and the rate in the Babushkin gauge is already close to convergent, the value $A_2 = 4.31(87) \times 10^{-7}\ \mathrm{s}^{-1}$ is used to represent the decay rate of this channel. The uncertainty is given as the difference between the rates in the two gauges. As a result, the lifetime of the metastable state is determined to be 26.5(5.3) days.

The resonant photon-excitation cross section [47] from the ground state to this metastable state is calculated to be $8.3 \times 10^{-14}\ \mathrm{cm}^2$ per photon. Current XUV frequency combs at such photon energy would have a repetition rate of 100 MHz and a pulse duration of 24 fs [48]. With proper phase-matching schemes, XUV combs with powers at the mW level are achievable [49]. Assuming an average power of 5 mW per harmonic or 25.5 nW per tooth and a focal size of 10 $\mu\mathrm{m}^2$, they bear a photon flux of $5.0 \times 10^{16}\ \mathrm{ph/s/cm}^2$ per tooth. Assuming a comb coherence time of 1 s [50], i.e., a tooth width of 160 mHz, the resonant photon flux would be $2.2 \times 10^{10}\ \mathrm{ph/s/cm}^2$. Thus, one would obtain 1.8×10^{-3} excitations per second (or an effective Rabi frequency of $\Omega/2\pi = 6.8$ mHz) at resonance [18], rendering future XUV resonant spectroscopy of this clock state promising. Nevertheless, before direct excitation of the metastable state, further spectroscopy of the nearby fast transitions such as $^4P_{5/2} \rightarrow {}^4G_{7/2}$, $^4G_{7/2} \rightarrow {}^4G_{9/2}$, and $^4G_{9/2} \rightarrow {}^2H_{11/2}$ is necessary to improve the accuracy of the clock transition energy to around 21 kHz. For the quantum logic scheme, however, one needs to be able to drive a sideband coupling in the HCI, whose Rabi frequency is typically smaller by a factor of $\eta = kz_0$. Here, η is the Lamb-Dicke parameter, k the wave number of the laser, and z_0 the spatial spread of the ground state motional wave function along the laser propagation direction [51]. Therefore, in order to realize the full ability of quantum logic, one needs to either increase the laser power or the coherence time of the XUV comb.

We have shown the experimental determination and theoretical calculation of the excitation energy of a low-lying metastable state in Pb^{41+}. The metastable $[\mathrm{Kr}]4d^5\ ^2H_{11/2}$ state and its most probable decay channels including the transition rates, calculated with the MCDHF1 method, are shown in Fig. 2, and the region of interest around the metastable state is enlarged to show the different values of experiment (PENTATRAP) and theory (MCDHF1 and 2). As can be seen, the calculation of MCDHF1 and MCDHF2 agree with the experimental data within 1σ. This comparison verifies the theoretical multi-electron correlation studies and excitation energy estimations described in this Letter. It also shows the ability of Penning-trap mass measurements to help in the search for transitions usable in future HCI clocks and to determine their energy at a sub-eV precision.

As described, the energy of the metastable state falls into the range of current XUV combs, allowing resonant spectroscopy of this metastable state using a high flux, high repetition rate XUV comb [16]. The orders-of-magnitude higher transition energy of XUV in comparison to optical clocks could enable the construction of an ultrastable clock with a fractional frequency instability around $4 \times 10^{-20}/\sqrt{\tau}$.

This work comprises parts of the Ph.D. thesis work of K. K. to be submitted to Heidelberg University, Germany. This work is part of and funded by the Max-Planck-Gesellschaft and the DFG (German Research Foundation)—Project-ID 273811115—SFB 1225 ISOQUANT. The project received funding from the European Research Council (ERC) under the European Union's Horizon 2020 research and innovation programme under grant agreement No. 832848—FunI. P. I., Y. N., and K. B. are members of the Allianz Program of the Helmholtz Association, Contract No. EMMI HA-216 "Extremes of Density and Temperature: Cosmic Matter in the Laboratory." Furthermore, we acknowledge funding and support by the International Max-Planck Research School for Precision Tests of Fundamental Symmetries and the Max Planck, RIKEN, PTB Center for Time, Constants and Fundamental Symmetries. The authors thank J. R. Crespo López-Urrutia and his team for insightful discussions and support. P. I. acknowledges support from CNRS and from the "Programme Hubert Curien PESSOA 47863UE."

*Corresponding author: kromer@mpi-hd.mpg.de

[1] J. L. Hall, Nobel Lecture: Defining and measuring optical frequencies, Rev. Mod. Phys. **78**, 1279 (2006).
[2] T. W. Hänsch, Nobel Lecture: Passion for precision, Rev. Mod. Phys. **78**, 1297 (2006).
[3] N. Huntemann, C. Sanner, B. Lipphardt, C. Tamm, and E. Peik, Single-ion atomic clock with 3×10^{-18} systematic uncertainty, Phys. Rev. Lett. **116**, 063001 (2016).

[4] S. Brewer, J.-S. Chen, A. Hankin, E. Clements, C. Chou, D. Wineland, D. Hume, and D. Leibrandt, $^{27}Al^{+}$ quantum-logic clock with a systematic uncertainty below 10^{-18}, Phys. Rev. Lett. **123**, 033201 (2019).

[5] X. Zheng, J. Dolde, V. Lochab, B. N. Merriman, H. Li, and S. Kolkowitz, Differential clock comparisons with a multiplexed optical lattice clock, Nature (London) **602**, 425 (2022).

[6] T. Bothwell, C. J. Kennedy, A. Aeppli, D. Kedar, J. M. Robinson, E. Oelker, A. Staron, and J. Ye, Resolving the gravitational redshift across a millimetre-scale atomic sample, Nature (London) **602**, 420 (2022).

[7] E. R. Clements, M. E. Kim, K. Cui, A. M. Hankin, S. M. Brewer, J. Valencia, J.-S. Chen, C.-W. Chou, D. R. Leibrandt, and D. B. Hume, Lifetime-limited interrogation of two independent $^{27}Al^{+}$ clocks using correlation spectroscopy, Phys. Rev. Lett. **125**, 243602 (2020).

[8] J. D. Prestage, R. L. Tjoelker, and L. Maleki, Atomic clocks and variations of the fine structure constant, Phys. Rev. Lett. **74**, 3511 (1995).

[9] R. Godun, P. Nisbet-Jones, J. Jones, S. King, L. Johnson, H. Margolis, K. Szymaniec, S. Lea, K. Bongs, and P. Gill, Frequency ratio of two optical clock transitions in $^{171}Yb^{+}$ and constraints on the time variation of fundamental constants, Phys. Rev. Lett. **113**, 210801 (2014).

[10] R. Lange, N. Huntemann, J. M. Rahm, C. Sanner, H. Shao, B. Lipphardt, Chr. Tamm, S. Weyers, and E. Peik, Improved limits for violations of local position invariance from atomic clock comparisons, Phys. Rev. Lett. **126**, 011102 (2021).

[11] C. Gohle, T. Udem, M. Herrmann, J. Rauschenberger, R. Holzwarth, H. A. Schuessler, F. Krausz, and T. W. Hänsch, A frequency comb in the extreme ultraviolet, Nature (London) **436**, 234 (2005).

[12] R. J. Jones, K. D. Moll, M. J. Thorpe, and J. Ye, Phase-coherent frequency combs in the vacuum ultraviolet via high-harmonic generation inside a femtosecond enhancement cavity, Phys. Rev. Lett. **94**, 193201 (2005).

[13] I. Pupeza, C. Zhang, M. Högner, and J. Ye, Extreme-ultraviolet frequency combs for precision metrology and attosecond science, Nat. Photonics **15**, 175 (2021).

[14] H. Carstens, M. Högner, T. Saule, S. Holzberger, N. Lilienfein, A. Guggenmos, C. Jocher, T. Eidam, D. Esser, V. Tosa, V. Pervak, J. Limpert, A. Tünnermann, U. Kleineberg, F. Krausz, and I. Pupeza, High-harmonic generation at 250 MHz with photon energies exceeding 100 eV, Optica **3**, 366 (2016).

[15] I. Pupeza, S. Holzberger, T. Eidam, H. Carstens, D. Esser, J. Weitenberg, P. Rußbüldt, J. Rauschenberger, J. Limpert, T. Udem, A. Tünnermann, T. W. Hänsch, A. Apolonski, F. Krausz, and E. Fill, Compact high-repetition-rate source of coherent 100 eV radiation, Nat. Photonics **7**, 608 (2013).

[16] T. Saule, S. Heinrich, J. Schötz, N. Lilienfein, M. Högner, O. deVries, M. Plötner, J. Weitenberg, D. Esser, J. Schulte, P. Russbueldt, J. Limpert, M. F. Kling, U. Kleineberg, and I. Pupeza, High-flux ultrafast extreme-ultraviolet photoemission spectroscopy at 18.4 MHz pulse repetition rate, Nat. Commun. **10**, 458 (2019).

[17] J. R. Crespo López-Urrutia, Frequency metrology using highly charged ions, J. Phys. Conf. Ser. **723**, 012052 (2016).

[18] C. Lyu, S. M. Cavaletto, C. H. Keitel, and Z. Harman, Interrogating the temporal coherence of EUV frequency combs with highly charged ions, Phys. Rev. Lett. **125**, 093201 (2020).

[19] C. Lyu, Z. Harman, and C. H. Keitel, Ultrastable optical, XUV and soft-x-ray clock transitions in open-shell highly charged ions, arXiv:2305.09603.

[20] P. Micke, T. Leopold, S. A. King, E. Benkler, L. J. Spieß, L. Schmöger, M. Schwarz, J. R. Crespo López-Urrutia, and P. O. Schmidt, Coherent laser spectroscopy of highly charged ions using quantum logic, Nature (London) **578**, 60 (2020).

[21] S. A. King, L. J. Spieß, P. Micke, A. Wilzewski, T. Leopold, E. Benkler, R. Lange, N. Huntemann, A. Surzhykov, V. A. Yerokhin, J. R. Crespo López-Urrutia, and P. O. Schmidt, An optical atomic clock based on a highly charged ion, Nature (London) **611**, 43 (2022).

[22] M. G. Kozlov, M. S. Safronova, J. R. Crespo López-Urrutia, and P. O. Schmidt, Highly charged ions: Optical clocks and applications in fundamental physics, Rev. Mod. Phys. **90**, 045005 (2018).

[23] V. I. Yudin, A. V. Taichenachev, and A. Derevianko, Magnetic-dipole transitions in highly charged ions as a basis of ultraprecise optical clocks, Phys. Rev. Lett. **113**, 233003 (2014).

[24] R. X. Schüssler, H. Bekker, M. Braß, H. Cakir, J. R. Crespo López-Urrutia, M. Door, P. Filianin, Z. Harman, M. W. Haverkort, W. J. Huang, P. Indelicato, C. H. Keitel, C. M. König, K. Kromer, M. Müller, Y. N. Novikov, A. Rischka, C. Schweiger, S. Sturm, S. Ulmer, S. Eliseev, and K. Blaum, Detection of metastable electronic states by Penning trap mass spectrometry, Nature (London) **581**, 42 (2020).

[25] D. Matei, T. Legero, S. Häfner, C. Grebing, R. Weyrich, W. Zhang, L. Sonderhouse, J. Robinson, J. Ye, F. Riehle, and U. Sterr, 1.5 μm lasers with Sub-10 mHz linewidth, Phys. Rev. Lett. **118**, 263202 (2017).

[26] P. Micke, S. Kühn, L. Buchauer, J. R. Harries, T. M. Bücking, K. Blaum, A. Cieluch, A. Egl, D. Hollain, S. Kraemer, T. Pfeifer, P. O. Schmidt, R. X. Schüssler, Ch. Schweiger, T. Stöhlker, S. Sturm, R. N. Wolf, S. Bernitt, and J. R. Crespo López-Urrutia, The Heidelberg compact electron beam ion traps, Rev. Sci. Instrum. **89**, 063109 (2018).

[27] Ch. Schweiger, C. M. König, J. R. Crespo López-Urrutia, M. Door, H. Dorrer, Ch. E. Düllmann, S. Eliseev, P. Filianin, W. Huang, K. Kromer, P. Micke, M. Müller, D. Renisch, A. Rischka, R. X. Schüssler, and K. Blaum, Production of highly charged ions of rare species by laser-induced desorption inside an electron beam ion trap, Rev. Sci. Instrum. **90**, 123201 (2019).

[28] H. S. W. Massey and D. R. Bates, The properties of neutral and ionized atomic oxygen and their influence on the upper atmosphere, Rep. Prog. Phys. **9**, 62 (1942).

[29] N. E. Bradbury and R. A. Nielsen, Absolute values of the electron mobility in hydrogen, Phys. Rev. **49**, 388 (1936).

[30] K. Kromer, C. Lyu, M. Door, P. Filianin, Z. Harman, J. Herkenhoff, W. Huang, C. H. Keitel, D. Lange, Y. N. Novikov, C. Schweiger, S. Eliseev, and K. Blaum, High-precision mass measurement of doubly magic ^{208}Pb, Eur. Phys. J. A **58**, 202 (2022).

[31] J. Repp, C. Böhm, J. R. Crespo López-Urrutia, A. Dörr, S. Eliseev, S. George, M. Goncharov, Y. N. Novikov, C. Roux, S. Sturm, S. Ulmer, and K. Blaum, PENTATRAP: A novel cryogenic multi-Penning-trap experiment for high-precision mass measurements on highly charged ions, Appl. Phys. B **107**, 983 (2012).

[32] C. Roux, C. Böhm, A. Dörr, S. Eliseev, S. George, M. Goncharov, Y. N. Novikov, J. Repp, S. Sturm, S. Ulmer, and K. Blaum, The trap design of PENTATRAP, Appl. Phys. B **107**, 997 (2012).

[33] L. S. Brown and G. Gabrielse, Precision spectroscopy of a charged particle in an imperfect Penning trap, Phys. Rev. A **25**, 2423 (1982).

[34] X. Feng, M. Charlton, M. Holzscheiter, R. A. Lewis, and Y. Yamazaki, Tank circuit model applied to particles in a Penning trap, J. Appl. Phys. **79**, 8 (1996).

[35] E. A. Cornell, R. M. Weisskoff, K. R. Boyce, and D. E. Pritchard, Mode coupling in a Penning trap: π pulses and a classical avoided crossing, Phys. Rev. A **41**, 312 (1990).

[36] E. A. Cornell, R. M. Weisskoff, K. R. Boyce, R. W. Flanagan, G. P. Lafyatis, and D. E. Pritchard, Single-ion cyclotron resonance measurement of $M(CO^+)/M(N_2^+)$, Phys. Rev. Lett. **63**, 1674 (1989).

[37] A. Rischka, H. Cakir, M. Door, P. Filianin, Z. Harman, W. Huang, P. Indelicato, C. Keitel, C. König, K. Kromer, M. Müller, Y. Novikov, R. Schüssler, C. Schweiger, S. Eliseev, and K. Blaum, Mass-difference measurements on heavy nuclides with an eV/c^2 accuracy in the PENTATRAP spectrometer, Phys. Rev. Lett. **124**, 113001 (2020).

[38] P. Filianin, C. Lyu, M. Door, K. Blaum, W. Huang, M. Haverkort, P. Indelicato, C. Keitel, K. Kromer, D. Lange, Y. Novikov, A. Rischka, R. Schüssler, C. Schweiger, S. Sturm, S. Ulmer, Z. Harman, and S. Eliseev, Direct Q-value determination of the β^- decay of ^{187}Re, Phys. Rev. Lett. **127**, 072502 (2021).

[39] S. Rau, F. Heiße, F. Köhler-Langes, S. Sasidharan, R. Haas, D. Renisch, C. E. Düllmann, W. Quint, S. Sturm, and K. Blaum, Penning trap mass measurements of the deuteron and the HD + molecular ion, Nature (London) **585**, 43 (2020).

[40] I. P. Grant, Relativistic calculation of atomic structures, Adv. Phys. **19**, 747 (1970).

[41] J. P. Desclaux, D. F. Mayers, and F. O'Brien, Relativistic atomic wave functions, J. Phys. B **4**, 631 (1971).

[42] C. F. Fischer, G. Gaigalas, P. Jönsson, and J. Bieroń, GRASP2018—a fortran 95 version of the general relativistic atomic structure package, Comput. Phys. Commun. **237**, 184 (2019).

[43] P. Indelicato and J. Desclaux, MCDFGME: A multiconfiguration Dirac–Fock and general matrix elements program (2005), http://www.lkb.upmc.fr/metrologysimplesystems/mdfgme-a-general-purpose-multiconfiguration-dirac-foc-program/.

[44] P. Indelicato, O. Gorveix, and J. P. Desclaux, Multiconfigurational Dirac-Fock studies of two-electron ions. II. Radiative corrections and comparison with experiment, J. Phys. B **20**, 651 (1987).

[45] P. Indelicato and J. P. Desclaux, Multiconfiguration Dirac-Fock calculations of transition energies with QED corrections in three-electron ions, Phys. Rev. A **42**, 5139 (1990).

[46] V. M. Shabaev, I. I. Tupitsyn, and V. A. Yerokhin, Model operator approach to the Lamb shift calculations in relativistic many-electron atoms, Phys. Rev. A **88**, 012513 (2013).

[47] C. J. Foot, *Atomic Physics* (Oxford University Press, Oxford, 2004), Vol. 7.

[48] J. Nauta, J.-H. Oelmann, A. Borodin, A. Ackermann, P. Knauer, I. S. Muhammad, R. Pappenberger, T. Pfeifer, and J. R. C. López-Urrutia, XUV frequency comb production with an astigmatism-compensated enhancement cavity, Opt. Express **29**, 2624 (2021).

[49] G. Porat, C. M. Heyl, S. B. Schoun, C. Benko, N. Dörre, K. L. Corwin, and J. Ye, Phase-matched extreme-ultraviolet frequency-comb generation, Nat. Photonics **12**, 387 (2018).

[50] C. Benko, T. K. Allison, A. Cingöz, L. Hua, F. Labaye, D. C. Yost, and J. Ye, Extreme ultraviolet radiation with coherence time greater than 1 s, Nat. Photonics **8**, 530 (2014).

[51] D. Wineland, C. Monroe, W. Itano, D. Leibfried, B. King, and D. Meekhof, Experimental issues in coherent quantum-state manipulation of trapped atomic ions, J. Res. Natl. Inst. Stand. Technol. **103**, 259 (1998).